An Experimental Study on the Image-Based Atmospheric Correction Using Multispectral Data

Kwang-Jae Lee
Korea Aerospace Research Institute
45 Eoeun-dong, Yuseong-gu, Daejeon, 305-333, Korea
kjlee@kari.re.kr

Yong-Seung Kim
Korea Aerospace Research Institute
45 Eoeun-dong, Yuseong-gu, Daejeon, 305-333, Korea
yskim@kari.re.kr

Abstract: The purpose of this study is to examine the image-based atmospheric correction models using the data from Landsat Enhanced Thermal Mapper Plus (ETM+) that have quite similar spectral characteristics to the forthcoming Korea Multi-Purpose SATellite (KOMPSAT)-2 Multi-Spectral Camera (MSC), and the *in-situ* measured surface reflectance data during satellite overflight. The main advantage of this type of correction is that it does not require *in-situ* measurements during each satellite overflight. While substantial differences are present between Top-Of-the Atmosphere (TOA) reflectance and *in-situ* measurements, the results showed that Case 1 based on COST model gives most accurate results among three cases. The accuracy of Case 2 is very close to Case 1 and its values are smaller than *in-situ* data. No notable features appear between some bands in the Case 3 and *in-situ* data. It is expected from this study that if the current methods are applied to the IKONOS high resolution data, we will be able to develop the suitable atmospheric correction methods for MSC data.

Keywords: KOMPSAT, MSC, Atmospheric Correction, Surface Reflectance.

1. Introduction

Digital analysis of remote sensing data has become an important component of a wide variety of earth science studies. Also remote sensing data have been used for various earth science applications, such as geology, mapping, atmosphere, ocean, environment, etc. Moreover, a major benefit of multi-temporal remote sensing data is its applicability to change detection (Robinove et al., 1981; Jensen and Toll, 1982; Fung, 1990; Chavez and MacKinnon, 1994). However, in order to fully realize the potential of spectral data for such application, it is necessary to convert satellite recorded digital counts to values independent of atmospheric conditions, that is, values of surface reflectance. Typical ways to correct for atmospheric effects is to use *in-situ* atmospheric measurements and radiative transfer code (RTC) (Chavez, 1996). However, the problem of this type of correction is that it requires *in-situ* field measurements during satellite overflight. Ideally, a model that utilizes ground truth data is the most accurate in terms of correction for atmospheric effects. However, in the most case, data users have to utilize the remote sensing data that have already been collected and archived. In this case, the simple Dark Object Subtraction (DOS) technique may be useful because it requires only information contained in the image data. Most DOS techniques assume that there is a high probability that there are at least a few pixels within an image which should be black (0% reflectance), thus the digital image system should not detect any radiance at dark shadow areas, and a DN value of zero should be assigned to them. However, these shadow areas will not be completely dark, because of atmospheric effects. For that reason, minimum DN values are subtracted in all bands so that zero values appear in the data, the effects of atmospheric scattering will be somewhat minimized. This simple DOS technique has been utilized for the past few decades (Vincent, 1972; Chavez, 1975, Rowan et al., 1974, etc). An improved DOS model proposed by Chavez in 1988 and 1989 is based on the assumption, that a completely black or zero reflectance surfaces usually does not exist and a minimum reflectance value of 1 or 2 percent is more realistic, was utilized for many applications. However, when this model was evaluated with low-altitude, aircraft-based measurements for seven dates over a 1 year period by Moran et al. (1992), it produced greater error in estimates of NIR reflectance than no correction at all. After her announcement, Chavez (1996) presented an entirely images-based procedure that expanded on the DOS model (COST model) by including a simple multiplicative correction for transmittance using published and unpublished data from Moran et al. (1992). In the results, the COST model which is atmospheric transmittance along the path from the sun to the ground surface generated results as good as the Herman-Browning Code (HBC) model.

In this study, we examined the image-based atmospheric correction models using the data from Landsat ETM+ that have quite similar spectral characteristics to the forthcoming KOMPSAT-2 MSC and the *in-situ* measured surface reflectance data during satellite overflight. KOMPSAT-2 MSC is scheduled to be launched in 2005, and expected to provide 1 m panchromatic image and 4 m multi-spectral image with four bands.

2. Data and Methods

To examine the image-based atmospheric correction

Landsat ETM+ data obtained on 22 November 2002 was utilized. Fig. 1 shows our study area. 22 ground control points (GCPs) extracted from the digital map of 1:25,000 and 13 radiometric targets were utilized for geometric correction and *in-situ* field measurements.

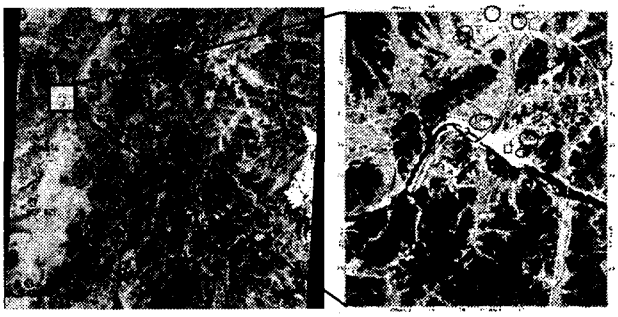

Fig. 1. Landsat ETM+ image (November 22, 2002) and 22 GCP extracted from the digital map of 1:25,000 (left) and location of *in-situ* measurement (right).

FR Portable Spectroradiometer (FieldSpec FR) was utilized to collect the field spectral data during Landsat ETM+ overflight. This instrument collects data from 350nm to 2500nm (Table 1), but we only used data from 450nm to 900nm for this study (Fig. 2). Also only the six field spectral data were used for this study because some field targets did not satisfy Landsat ETM+ spatial resolution. Fig. 2 shows the results of *in-situ* measured surface that was average of five times. These data were obtained from Korea Institute of Geoscience & Mineral Resources (KIGAM). *In-situ* field measurements are used to evaluate the accuracy of each method that computes the surface reflectance from the ETM+ satellite image.

Table 1. FieldSpec FR specification.

Spectral Bandwidth	1.4㎚ in the 350㎚ to 1000㎚ 2.0㎚ in the 1000㎚ to 2500㎚
Spectral Range	350㎚ to 2500㎚
Spectral Resolution	2㎚@700㎚, 10㎚@1500㎚, and 10㎚@2100㎚
Sensor Linearity	±1%
Wavelength Accuracy	±1%
Scan Time	A new spectrum is generated every 0.1 seconds for the entire spectral range
Operational Weight	7kg+2.2kg battery pack
Operational Size	35×29×13㎝

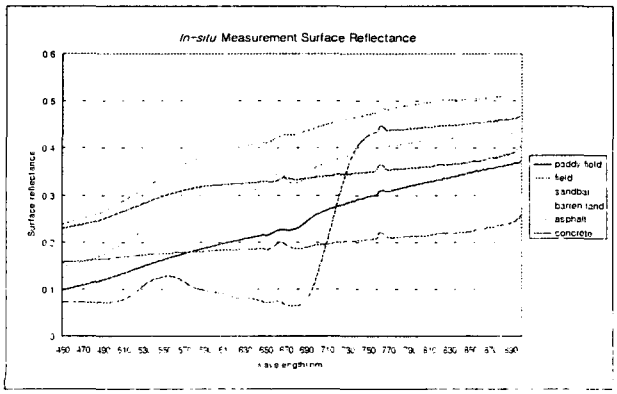

Fig. 2. The measured surface reflectance from six different targets using FieldSpec FR (KIGAM, 2002).

Three approaches have been experimented in this study; each of which calculates surface reflectance from Equation (1) using different assumptions for T_v^{dir}, T_v^{diff}, T_z^{dir}, and T_z^{diff} (Table 2).

$$\rho_{surface} = \frac{\pi(L_{sat} - L_{path})}{T_v(E_{sun}\cos(\theta_z)T_z + E_{down})} =$$

$$\rho_{surface} = \frac{\pi(L_{sat} - L_{path})}{T_v E_{sun}\cos(\theta_z)(T_z^{dir} + T_z^{diff})} \quad (1)$$

Where,

L_{sat} Spectral radiance at the satellite sensor.

L_{path} Unwelling atmospheric spectral radiance scattered in the direction of and at the sensor entrance pupil and within the sensor's field of view, i.e., the path radiance.

E_{sun} Solar spectral irradiance on a surface perpendicular to the sun's rays outside the atmosphere. E_{sun} contains the correction of the earth-sun distance.

T_v Atmospheric transmittance along the path from the ground surface to the sensor $(T_z^{dir} + T_v^{diff})$.

T_z Atmospheric transmittance along the path from the sun to the ground surface.

θ_z Angle of incidence of the direct solar flux onto the earth's surface. Downwelling spectral irradiance at the surface due to the scattered solar flux in the atmosphere.

The path radiance (L_{path}) was assumed to be the dark-object radiance minus the radiance contributed by 0.01 surface reflectance. These path radiance values were used to do a dark-object subtraction correction.

Table 2. Each transmittance value for three cases used in Equation (1).

Method	T_v^{dir}	T_v^{diff}	T_z^{dir}	T_z^{diff}
Case 1	1	0	$\cos(\theta_z)$	0
Case 2	1	0	$\cos(\theta_z)$	$\tau_{T_z^{dir}}$ $\tau_{T_z^{dir}}$ $\tau_{T_z^{dir}}$
Case 3	$e^{-\tau/\cos\theta_z}$	$\tau_{T_z^{dir}}$ $\tau_{T_z^{dir}}$ $\tau_{T_z^{dir}}$	$e^{-\tau/\cos\theta_z}$	$\tau_{T_z^{dir}}$ $\tau_{T_z^{dir}}$ $\tau_{T_z^{dir}}$

Three approaches in this study are based on the COST model, and Table 3 is estimated results from Cess *et al.* (1991) and Sohn *et al.* (1998).

Table 3. Estimates of aerosol, Rayleigh and total optical thickness used for this study ($\tau_{0.5um} = 0.4$).

Landsat ETM+	Aerosol(τ_{Aer})	Rayleigh(τ_{Ray})	Total
τ_{band1}	0.4×1.24=0.496	0.226	0.722
τ_{band1}	0.4×1=0.4	0.099	0.499
τ_{band1}	0.4×0.81=0.324	0.050	0.374

τ_{band1}	0.4×0.65=0.26	0.023	0.283

3. Results and Discussion

Table 4 shows the results of surface reflectance factors that were computed using three approaches. The RMS error in Fig. 3 is the standard deviation of the difference between the satellite-based estimates and *in-situ* measurements of surface reflectance. The scatter plot (Fig. 3) and Table 4, while substantial difference are present between TOA reflectance and *in-situ* measurements, the results showed that Case 1 based on COST model gives most accurate results among three cases. The accuracy of Case 2_1 is very close to Case 1 and its values are smaller than *in-situ* data. No notable features appear between some bands in the Case 3_1 and *in-situ* data.

Table 4. Estimates of surface reflectance for six different targets using Landsat ETM+ data.

ETM+	Case	Paddy field	Field	Sand bar	Barren land	asphalt	Concrete
Band1	DN	71	67	90	78	68	78
	TOA	0.146	0.137	0.191	0.163	0.139	0.163
	Case 1	0.126	0.108	0.211	0.158	0.113	0.158
	Case 2_1	0.103	0.089	0.171	0.128	0.092	0.128
	Case 2_2	0.097	0.084	0.161	0.121	0.087	0.121
	Case 2_3	0.088	0.076	0.144	0.108	0.079	0.108
	Case 3_1	0.330	0.280	0.563	0.416	0.293	0.416
	Case 3_2	0.291	0.240	0.496	0.366	0.258	0.366
	Case 3_3	0.232	0.198	0.394	0.292	0.206	0.292
	Measured	0.117	0.072	0.260	0.168	0.163	0.245
Band2	DN	56	53	88	71	53	68
	TOA	0.122	0.115	0.204	0.161	0.115	0.153
	Case 1	0.152	0.138	0.310	0.226	0.138	0.211
	Case 2_1	0.124	0.112	0.250	0.183	0.112	0.171
	Case 2_2	0.117	0.106	0.235	0.172	0.106	0.161
	Case 2_3	0.105	0.095	0.210	0.154	0.095	0.144
	Case 3_1	0.214	0.193	0.439	0.319	0.193	0.298
	Case 3_2	0.189	0.171	0.387	0.282	0.171	0.263
	Case 3_3	0.151	0.137	0.308	0.225	0.137	0.210
	Measured	0.170	0.127	0.354	0.268	0.178	0.305
Band3	DN	66	57	109	89	53	84
	TOA	0.136	0.115	0.238	0.191	0.106	0.179
	Case 1	0.219	0.178	0.413	0.323	0.160	0.300
	Case 2_1	0.177	0.144	0.333	0.260	0.130	0.242
	Case 2_2	0.166	0.136	0.313	0.245	0.122	0.228
	Case 2_3	0.149	0.122	0.279	0.219	0.110	0.203
	Case 3_1	0.217	0.177	0.411	0.321	0.159	0.298
	Case 3_2	0.192	0.156	0.362	0.283	0.141	0.263
	Case 3_3	0.154	0.126	0.288	0.226	0.113	0.210
	Measured	0.222	0.074	0.420	0.337	0.192	0.330
Band4	DN	61	61	90	79	49	76
	TOA	0.191	0.191	0.295	0.256	0.148	0.245
	Case 1	0.336	0.336	0.537	0.461	0.253	0.440
	Case 2_1	0.271	0.271	0.431	0.370	0.204	0.354
	Case 2_2	0.254	0.254	0.405	0.348	0.192	0.332
	Case 2_3	0.227	0.227	0.361	0.310	0.172	0.297
	Case 3_1	0.258	0.258	0.411	0.353	0.195	0.337
	Case 3_2	0.228	0.228	0.362	0.311	0.172	0.297
	Case 3_3	0.182	0.182	0.288	0.248	0.138	0.237
	Measured	0.337	0.449	0.503	0.420	0.220	0.365

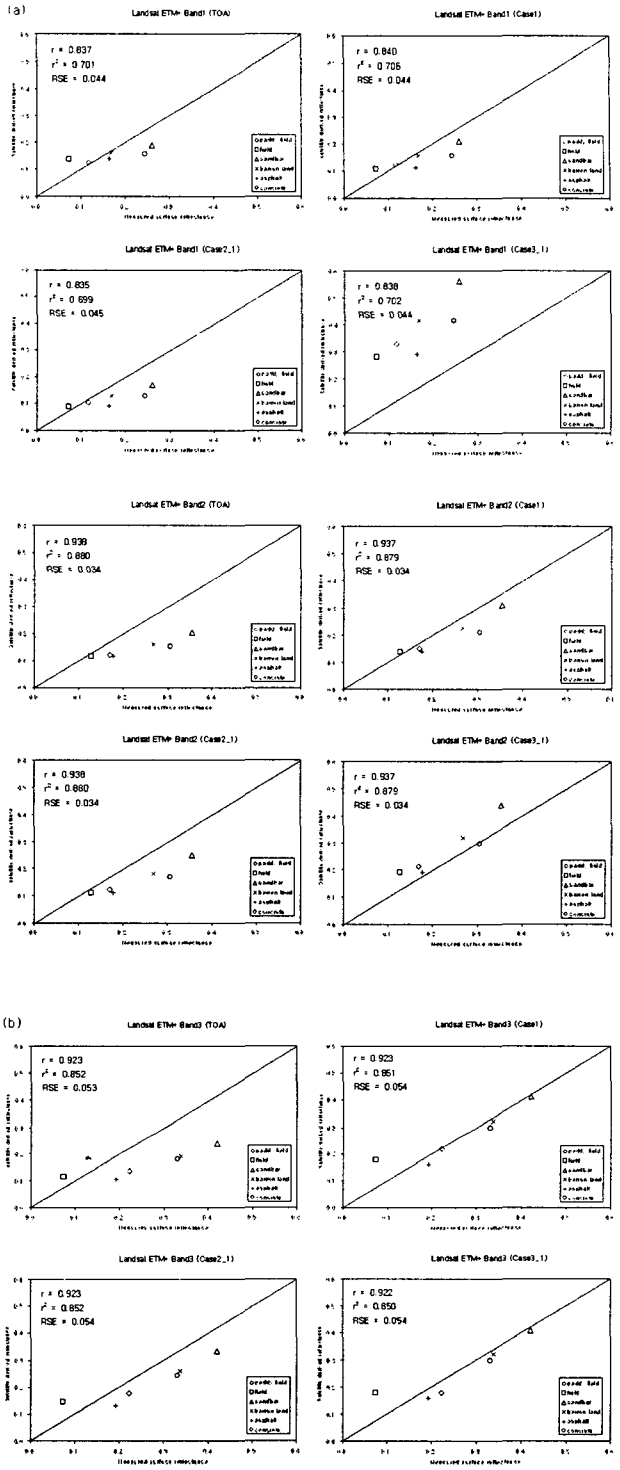

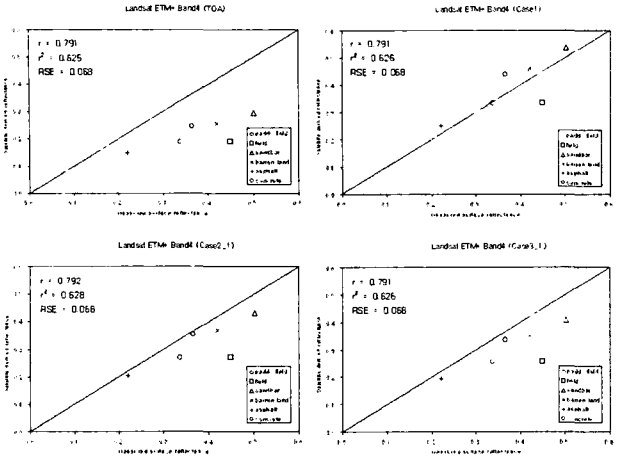

Fig. 3. Comparisons of satellite-derived reflectance and in-situ measurements for each band: (a) band 1 and band 2, (b) band 3 and band 4.

Fig. 4 and Fig. 5 are based on the results of Fig. 3, Fig. 4 and 5 show the results of comparison of TOA and Case 1 histogram distribution pattern and satellite-derived surface reflectance of Case 1 and Case 2_1 with measured surface reflectance.

It is expected from this study that if the current methods are applied to the IKONOS high resolution data, we will be able to develop the suitable atmospheric correction methods for MSC data.

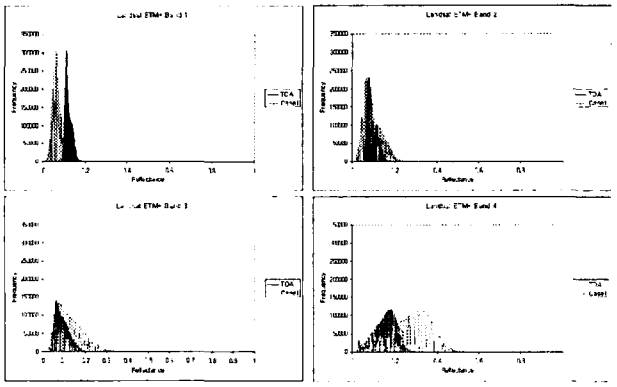

Fig. 4. A Comparison of TOA and Case 1 histogram distribution pattern.

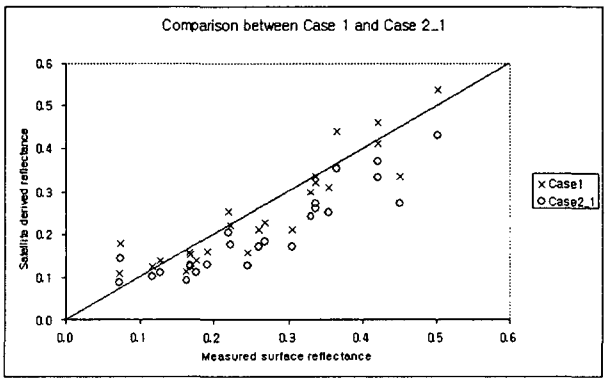

Fig. 5. Comparisons satellite-derived surface reflectance of Case 1 and Case 2_1 with measured surface reflectance.

4. Conclusions

Digital analysis of remote sensing data has become an important component of many earth science studies. Especially, surface reflectance is an important parameter to detect and monitor the global and environmental changes However, to maximize the benefit, multi-spectral data must be corrected with haze values that are spectral band dependent.

In this study, three cases were experimented to examine the image-based atmospheric correction model using Landsat ETM+ that has quite similar spectral characteristics to the forthcoming KOMPSAT-2 MSC and *in-situ* measurements of surface reflectance. The results showed that Case 1 based on COST model was the most accurate in terms of correction for atmospheric effects. However, since Case 2 accounts for more physical components and produces promising results comparable to Case 1, we need further studies for better performance of such model. Also off-nadir viewing corrections are needed for images subject to most passes of KOMPSAT-2.

Acknowledgement

This research was supported by Ministry of Science and Technology (MOST). *In-situ* measurement data were obtained from Korea Institute of Geoscience & Mineral Resources (KIGAM).

References

[1] Cess, R. D., E. G. Dutton, J. J. Deluisi, and F. Jiang, 1991 Determining surface solar absorption from broadband satellite measurements for clear skies: Comparison with surface measurements, *Journal of Climate*, pp.236-000.

[2] Chavez, P. S., Jr., 1975. Atmospheric, solar, and M.T.F. corrections for ERTS digital imagery, *Proc. American Society of Photogrammetry Fall Conference*, Phoenix, Arizona, p.69.

[3] Chavez, P. S., Jr., 1988. An improved dark-object subtraction technique for atmospheric scattering correction of multispectral data, *Remote Sensing of Environment*, 24:459-479.

[4] Chavez, P. S., Jr., 1989. Radiometric calibration of Landsat Thematic Mapper multispectral images, *Photogrammetric Engineering & Remote Sensing*, 55(9):1285-1294.

[5] Chavez, P. S., Jr., 1996. Image-based atmospheric corrections-Revisited and improved, *Photogrammetric Engineering & Remote Sensing*, 62(9):1025-1036.

[6] Chavez, P. S., Jr., and D. K. MacKinnon, 1994. Automatic detection of vegetation changes in the southwestern United States using remotely sensed images, *Photogrammetric Engineering & Remote Sensing*, 60(5):571-583.

[7] Cho, H. K., M. J. Jeong, J. H. Kim, and Y. J. Kim, 2003. Dependence of diffuse photosynthetically active solar irradiance on total optical depth, *Journal of Geophysical Research*, 108(9):1-10.

[8] Fung, T., 1990. An assessment of TM imagery for land-cover change detection, *IEEE transactions on Geoscience and Remote Sensing*, 28(4):681-684.

[9] Jensen, J. R., and D. L. Toll, 1982. Detecting residential land-use development at the urban fringe, *Photogrammet-*

ric Engineering & Remote Sensing, 48(4):629-643.

[10] Korea Institute of Geoscience & Mineral Resources, 2002. Public applications research of satellite data-construction of ground truth clearing house for land applications, *Annual report (1^{st})*, 228pp.

[11] Moran, M. S., R. D. Jackson, P. N. Slater, and P. M. Teillet, 1992. Evaluation of simplified procedures for retrieval of land surface reflectance factors from satellite sensor output, *Remote Sensing of Environment*, 41:169-184.

[12] Robinove, C. J., P. S. Chavez, Jr., D. Gehring, and R. Holmgrem, 1981. Arid land monitoring using Landsat albedo difference images, *Remote Sensing of Environment*, 11:133-156.

[13] Rowan, L. C., P. H. Wetlaufer, A. F. H. Goetz, F. C. Billingsley, and J. H. Stewart, 1974. Discrimination of rock types and detection of hydrothermally altered areas in south-central Nevada by the use of computer-enhanced ERTS images, *U.S. Geological Survey Professional Paper 883*, 35pp.

[14] Sohn, B. J., D. S. Shin, and S. S. Lee, 1998. Optical characteristics of the Yellow Sand from ground-based solar radiation measurements near the Yellow Sea, *Proc. ISRS'1998*, Korea, pp.9-13.

[15] Vincent, R. K., 1972. An ERTS multispectral scanner experiment for mapping iron compounds, *In proceedings of the Eighth International Symposium on Remote Sensing of Environment*, Ann Arbor, MI, pp.1239-1247.